Triaxial Deformation Behavior of Bituminous Mixes

E. A. Ossa[1]; V. S. Deshpande[2]; and D. Cebon[3]

Abstract: The triaxial compressive response of bituminous mixes with volume fractions of aggregate in the range 52 to 85% was investigated over a wide range stresses and strain rates. The types of loadings considered include triaxial monotonic constant stress and constant applied strain rate, as well as creep recovery, continuous cyclic, and stress pulse train loadings. The mixes with a "fully dense" aggregate skeleton were found to dilate under all loading conditions and the creep response of the mixes was dependent on both the deviatoric and hydrostatic stresses. By contrast, recovery was found to occur under zero applied deviatoric stresses with the recovery rate only dependent on the "recoverable strain" and independent of any superimposed hydrostatic stress. Continuous and pulse loading cyclic stress-controlled tests showed that the response of the mixes was governed by the mean applied deviatoric stress in the continuous cyclic tests while strain recovery was important in the pulse loading tests. A phenomenological constitutive model was proposed to fit the measured triaxial response of the bituminous mixes and shown to capture the measurements over all the triaxial stress states and loading time histories investigated here. Furthermore, the model was extended to capture the temperature dependence of the mixtures which is governed by the temperature dependence of the bitumen binder.

DOI: 10.1061/(ASCE)0899-1561(2010)22:2(124)

CE Database subject headings: Asphalts; Transient response; Cyclic tests; Deformation; Constitutive models; Triaxial tests; Bitumen.

Introduction

One of the most common forms of surface failure in flexible pavements is permanent deformation or *rutting*. Rutting is strongly influenced by the constitutive behavior of the bituminous mixes (asphalts) used in the upper layers of pavements. It is therefore necessary to understand the constitutive behavior of these materials in order to predict and prevent pavement rutting accurately.

The deformation behavior of a flexible pavement under a wheel load is strongly dependent on the multiaxial stress state in the pavement. The majority of the research investigating the constitutive response of asphalt has involved uniaxial compressive experimentation. Nevertheless triaxial testing has long been recognized as critical to understand the constitutive response of asphalt. For example, Huang (1967) discussed the limitations of using a linear viscoelastic theory to describe the mix behavior under multiaxial stress states and later Brown and Snaith (1974) and Brown and Cooper (1980) demonstrated via a series of triaxial tests that the response of asphalt was a function of both the hydrostatic and deviatoric stresses under monotonic and cyclic loadings.

A number of different approaches have been employed to develop constitutive models for bituminous mixes (or asphalt). These approaches include:

1. The application of the nonlinear correspondence principle of Schapery (1984) [see for example the works of Lee and Kim (1998) and Zhao and Kim (2003)];
2. The use of soil mechanics based theories, e.g., Nijboer (1948), Ramsamooj et al. (1998), and Deshpande and Cebon (1999);
3. Application of viscoelastic or viscoplastic models, e.g., Lytton et al. (1993), Long (2001), Huang et al. (2002), Collop et al. (2003), Huang et al. (2004), and Abbas et al. (2004); and
4. Discrete element models based on individual particle contacts [see for example, Hills and Heukelom (1969), Chang and Meegoda (1993), Cheung et al. (1999), and Zhu and Nodes (2000)].

These constitutive models often do not incorporate the dilatancy effects observed in experiments and typically only apply to the steady-state deformation behavior. Additionally, some of these models involve numerous fitting parameters that are determined from many calibration experiments: the large number of calibration tests makes these models difficult to use in practical design.

The aim of this study is to develop a simple phenomenological model for the multiaxial response of bituminous mixes under a wide range of loading conditions. Deshpande and Cebon (1999) and Collop and Khanzada (2001) have demonstrated that the rate dependence of bituminous mixes was similar to that of pure bitumen under both uniaxial and triaxial loading conditions. The main qualitative difference between the mixes and pure bitumen is the dilatancy of the mixes. In this study the phemomenological viscoplastic constitutive model for bitumen of Ossa et al. (2005) is extended to bituminous mixes.

The outline of the paper is as follows. First, triaxial compression experiments on bituminous mixes with volume fractions of aggregate in the range 52 to 85% are described. The experiments performed include monotonic constant strain-rate tests, constant

[1]Associate Professor, Engineering Materials Research Group, Dept. of Production Engineering, EAFIT Univ., Cra 49 Nr 7 sur 50, Medellin, Colombia.

[2]Reader in Mechanics of Materials, Dept. of Engineering, Cambridge Univ., Trumpington St., Cambridge CB2 1PZ, U.K.

[3]Professor of Mechanical Engineering, Dept. of Engineering, Cambridge Univ., Trumpington St., Cambridge CB2 1PZ, U.K. (corresponding author). E-mail: dc@eng.cam.ac.uk

Note. This manuscript was submitted on August 11, 2006; approved on May 7, 2009; published online on January 15, 2010. Discussion period open until July 1, 2010; separate discussions must be submitted for individual papers. This paper is part of the ***Journal of Materials in Civil Engineering***, Vol. 22, No. 2, February 1, 2010. ©ASCE, ISSN 0899-1561/2010/2-124–135/$25.00.

Table 1. Composition of the Mixes Investigated in This Study

Mix	Volume fraction of aggregate (%)	Volume fraction of voids (%)	Composition of aggregate
Mix A	52	≈3	Subspherical sand particles between 1.18 and 2.36 mm in size
Mix B	75	≈4	1. Subspherical sand particles between 300 and 600 μm in size (37.5%) 2. Subspherical sand particles between 1.8 and 2.36 mm in size (37.5%)
Mix C	85	≈4	1. Subspherical sand particles between 150 and 300 μm in size (11%) 2. Subspherical sand particles between 1.8 and 2.36 mm in size (18%) 3. Subspherical stones ~10 mm in diameter (56%)
Mix D	85	≈9	1. Subspherical sand particles between 150 and 300 μm in size (11%) 2. Subspherical sand particles between 1.8 and 2.36 mm in size (18%) 3. Angular stones ~10 mm (56%)

Note: The volume fraction of bitumen is calculated as the remaining to complete 100%. The volume fraction of voids refers to the voids between asphalt and coated particles.

stress creep tests, continuous stress-controlled cyclic tests, and stress pulse train experiments. The experiments were used to motivate a phenomenological multiaxial constitutive model for the bituminous mixes. Finally, comparisons of the predictions of the model with the measurements are presented.

Experimental Investigation

The main aim of this study was to explore the deformation behavior of bituminous mixes under monotonic and cyclic loadings over a range of axisymmetric compressive stress states. Mixes with volume fractions of aggregate varying from 52 to 85% were investigated; the microstructure and behavior of the low volume fraction mixes are not representative of asphalt but these experiments nevertheless help in giving a broad understanding of the effect of volume fraction of aggregate on the behavior of asphalt. The temperature dependence of the mixes of aggregate and bitumen is governed by the temperature dependence of the bitumen [see for example, Deshpande and Cebon (2000) and Ossa (2004)]. Thus, this study was restricted to investigating the effect of (1) volume fraction of sand; (2) stress triaxiality; and (3) loading conditions (e.g., cyclic versus monotonic) on the behavior of the mixes with all tests performed at room temperature (20°C).

Mix Specification

Pure Bitumen

A 50 penetration grade (pen) bitumen was employed in this study. [As the materials tested were not intended for a specific application, the penetration grade (pen) specified by the manufacturer is used to identify the bitumen instead of the performance grade (PG) specification.) This bitumen is commonly used in hot rolled asphalt paving mixtures as well as in coated Macadam paving mixtures in the United Kingdom (Whiteoak. 1990) and has been extensively characterized by Ossa et al. (2005) under uniaxial tensile monotonic and cyclic loadings over a wide range of temperatures.

Mixes

Four types of mixes comprising between 52 and 85% by volume aggregate were investigated in this study. The specifications of these mixes are listed in Table 1. Mixes B–D are fully dense sand and bitumen mixes, i.e., maximum aggregate volume fraction for that particular aggregate gradation. The maximum random packing densities for various particle size distributions are given in German (1989). By contrast, Mix A is a low fraction (52%) dispersion of sand in a bitumen matrix.

The mixes were manufactured as follows. A cylindrical mold was manufactured and used to cast and compact the specimens. The diameter of the cylinder was chosen so that it was at least seven times greater than the size of the largest aggregate particles and thus the Mixes A and B had specimens with diameter of 38.5 mm while 70-mm diameter specimens were employed for Mixes C and D. The ratio of the height to the diameter of the specimen was chosen to be around 2. A lubricant consisting of a mixture of natural soap and glycerin was applied to the inside surface of the mold to prevent sticking of the bituminous mixture. Compaction of the specimens was achieved by double plunger, with the surfaces of the plungers (top and bottom) lubricated with the same mixture of soap and glycerin [see Ossa (2004) for further details on the compaction technique].

Slightly different techniques were used to manufacture the fully dense Mixes B–D and the dispersoid, Mix A. The fully dense mixtures were made by heating together a mixture comprising the correct amounts of bitumen and aggregate. This mixture was then well stirred, transferred into the mold, and compacted in a mechanical press with a compaction pressure of about 10 MPa. The problem with preparing a specimen with an aggregate volume fraction less than the maximum random packing density is that the sand settles and separates from the bitumen when the mixture is heated. Hence a cold compaction technique was employed to manufacture specimens of Mix A [see Deshpande and Cebon (2000) and Ossa et al. (2004b) for details]. A brief description of the compaction technique will follow.

A cylindrical mold was manufactured with a diameter of 38.5 mm and a ratio of height to diameter of 2. A lubricant consisting of a mixture of natural soap and glycerine [see Cheung (1995)] was applied to the inner surface of the mold to avoid sticking of the mix. Crushed cold bitumen was mixed with the correct amount of sand (52% volume fraction) and then poured into the mold. The powdered mix was then compacted in a mechanical press (at room temperature) and then heated in a furnace for 1 h at 55°C (which was the softening temperature of the bitumen used). This soft mixture (still in the mold) was further compacted at 5 MPa for 5 min to allow the bitumen to fill the air voids and bond with the sand. The mold was then placed in a freezer to cool down the specimen to about 0°C. Finally, the cold specimen was slowly pushed out of the mold.

J. Mater. Civ. Eng., 2010, 22(2): 124-135

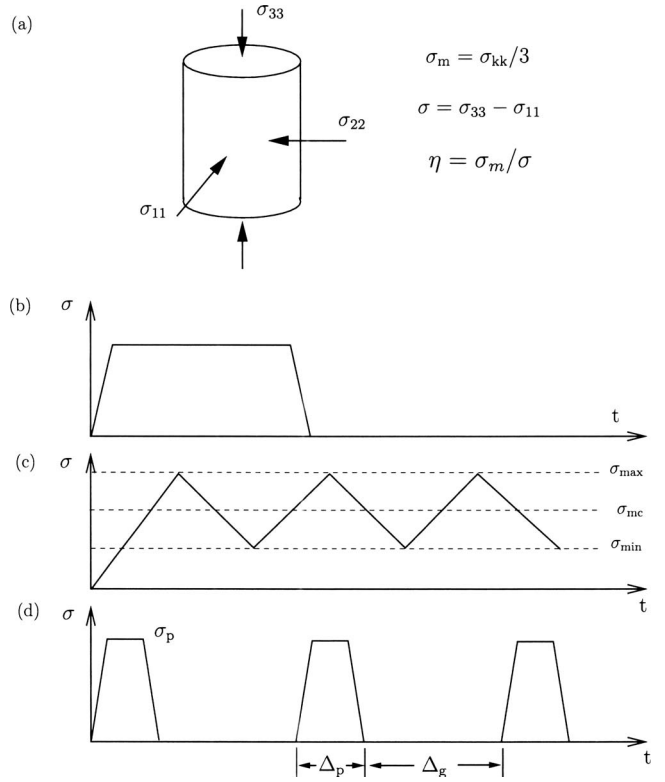

Fig. 1. Schematic showing the axisymmetric triaxial test coordinate system and test sequences. (a) Stresses on the cylindrical specimen and definition of the stress ratio η; (b) recovery test; (c) continuous cyclic test sequence; and (d) pulse train test sequence.

Description of Apparatus

A standard axisymmetric triaxial cell of the type commonly used in soil mechanics was used in the experimental investigation. It had a maximum allowable confining pressure of 1.5 MPa. The fluid used in the triaxial cell was derated water and the pressure was applied via a pump comprising a hydraulic actuator driven by a stepper motor. The axial load was applied by a hydraulic actuator with a submersible 10-kN load cell in the water employed to measure the axial applied load. This load cell was insensitive to the fluid pressure within the triaxial cell. The axial strain in the specimen was determined from the load line displacement of the hydraulic actuator. The radial strains of Mixes A and B were measured using a Hall effect radial transducer. The radial strains of specimens of Mixes C and D (85% volume fraction) were not measured in the triaxial tests because the diameter of the specimens was too large for the available transducer. The radial strains in these specimens were only measured in the uniaxial compression tests using a laser radial strain transducer.

A pressure transducer was fitted directly to the triaxial cell in order to monitor the applied confining pressure. The applied axial load, confining pressure, radial strains, and axial strains were measured as a function of time via a digital recording system.

Testing Procedure

The radial strain transducer was fitted on the specimen (Mixes A and B only) and the specimen was placed between the two compression platens (which were lubricated with a mixture of glycerine and natural soap to reduce friction and minimize bulging during the compression test) of the triaxial cell. The triaxial cell was then filled with water and the pressure controller set to maintain a fixed pressure. Note that the low volume fraction of voids in the specimens allowed the specimens to be pressurized directly by the water without any sealing; Deshpande and Cebon (1999) employed a similar method for their triaxial tests on idealized bituminous mixes.

Four types of tests were performed on these mixes: monotonic creep and constant applied strain-rate tests, creep recovery tests, continuous cyclic, and pulse stress-controlled tests. The test protocol for each of these tests is briefly described below. It is worth mentioning here that a number of spot repeat tests at each testing condition confirmed that the uncertainty of the results was below 10%. For the sake of brevity, these repeat results are not presented here [see Ossa (2004) for more details on the repeat tests performed].

Monotonic Tests

Two types of monotonic compression tests were performed. (1) Constant strain rate uniaxial compression experiments and (2) triaxial constant stress creep tests. In the constant strain-rate experiments a constant axial displacement rate ($\dot{\delta}=\dot{\varepsilon}l$) was applied to the cylindrical specimens and the resultant axial stress and strain recorded. The test protocol for the triaxial creep tests was as follows. After the target pressure P in the fluid was reached and stable, an axial load was applied instantaneously using a pulse wave form and maintained at that constant value. The axial load, axial displacement, radial strain, and hydrostatic pressure were logged for the duration of the test. The axial load Q and the fluid pressure P are related to the principal nominal stresses [see Fig. 1(a) for the definitions of the coordinate system] via

$$\sigma_{33} = Q/A + P$$

$$\sigma_{22} = P$$

$$\sigma_{11} = P \tag{1}$$

where A=circular cross-sectional area of the specimen. Thus, the mean stress σ_m and a measure of the deviatoric stress σ were

$$\sigma_m = \sigma_{kk}/3 = P + \frac{Q}{3A} \tag{2a}$$

$$\sigma = \sigma_{33} - \sigma_{11} = \frac{Q}{A} \tag{2b}$$

respectively. The tests were performed over a range of hydrostatic and deviatoric stresses. The stresses were applied such that for a particular constant stress triaxiality

$$\eta = \sigma_m/\sigma \tag{3}$$

the deviatoric stress σ was varied over approximately two orders of magnitude. The stress ratio η was varied from $\eta=1/3$ (uniaxial compression) to $\eta=1$ ($P=2Q/3A$).

Triaxial Creep Recovery Tests

The triaxial creep recovery behavior of the mixes was investigated by performing a series of single load/unload tests, under hydrostatic pressure. The applied deviatoric stress history is sketched in Fig. 1(b) and the test protocol was as follows. Once the target fluid pressure had been attained within the triaxial cell, a compressive axial load Q was applied rapidly and then held constant. The specimen was allowed to creep to a specified total nominal compressive axial strain ε_{33}^T. At this strain, the axial load

J. Mater. Civ. Eng., 2010, 22(2): 124-135

Q was released (keeping the fluid pressure P constant) and the compressive axial strain was monitored until it returned to $\dot{\varepsilon}_{33} \approx 0$. The axial strain at this point

$$\varepsilon_{33}^{\mathrm{pl}} = \varepsilon_{33}^{T} - \varepsilon_{33}^{r} \tag{4}$$

is the irrecoverable axial strain, with ε_{33}^{r} the axial strain recovered during the unloading phase. Note that in these tests, creep recovery occurred under a finite hydrostatic pressure but no deviatoric stress (in the uniaxial compression tests, creep recovery was under zero deviatoric and zero hydrostatic stress). Such tests were repeated for a series of axial strains ε_{33}^{T}, applied deviatoric stresses σ and stress ratios η.

Continuous Cyclic Tests

In the continuous cyclic triaxial tests, the axial load Q was varied between $Q_{\min}$ and $Q_{\max}$, while the fluid pressure P was held constant. The cyclic deviatoric stress was therefore varied between $\sigma_{\min}=Q_{\min}/A$ and $\sigma_{\max}=Q_{\max}/A$ as sketched in Fig. 1(c). These cyclic deviatoric stress levels define the deviatoric stress ratio and mean cyclic deviatoric stress as

$$R = \frac{\sigma_{\min}}{\sigma_{\max}} \tag{5a}$$

and

$$\sigma_{\mathrm{mc}} = \frac{\sigma_{\min} + \sigma_{\max}}{2} \tag{5b}$$

respectively. The deviatoric loading rate was governed by the frequency f of the triangular waveform. Note that as the fluid pressure P was kept constant in these tests, the stress triaxiality η varied between the minimum and maximum values

$$\eta_{\min} = \frac{P}{\sigma_{\max}} + \frac{1}{3} \tag{6a}$$

and

$$\eta_{\max} = \frac{P}{\sigma_{\min}} + \frac{1}{3} \tag{6b}$$

respectively, with a mean value of the stress triaxiality

$$\eta_m = \frac{\eta_{\min} + \eta_{\max}}{2} = \frac{P}{2}\left(\frac{1}{\sigma_{\min}} + \frac{1}{\sigma_{\max}}\right) + \frac{1}{3} \tag{7}$$

In these tests, the nominal axial strain was measured as a function of time and tests repeated for a series of values of R, f, σ_{mc}, and stress triaxiality η_m.

The ability of the pressure controller to maintain a constant pressure during the continuous cyclic tests was assessed via a series of preliminary tests. Over the load and frequency range investigated here, the pressure controller maintained the fluid pressure to within 2% of the target: this is considered satisfactory for the current experimental investigation.

Pulse Train Tests

Tests comprising intermittent identical compressive axial stress pulses with a trapezoidal shape in the time domain were performed in order to simulate a load history similar to that experienced in a pavement Fig. 1(d). The fluid pressure P was held constant as in the other tests. The aim here was to investigate the relationship between the single load/unload behavior analyzed via the creep and creep recovery tests, and the gradual racketing of strain due to the application of a continuous train of discrete stress pulses.

The trapezoidal deviatoric stress pulses were applied for a duration Δ_p with a stress amplitude σ_p and loading and unloading rate $\dot{\sigma}=4\sigma_p/\Delta_p$ [Fig. 1]. The stress triaxiality η_p in these tests is defined using the maximum deviatoric stress during the pulse as

$$\eta_p \equiv \frac{P}{\sigma_p} + \frac{1}{3} \tag{8}$$

Pulse stress tests were performed at selected stress triaxialities η_p and the time gap Δ_g between consecutive trapezoidal pulses was varied with the stress amplitude σ_p kept fixed.

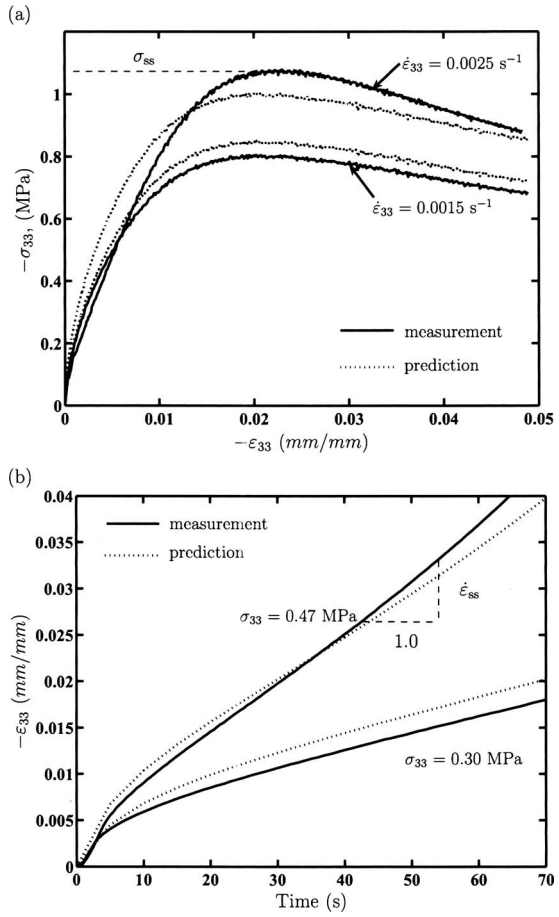

Fig. 2. Monotonic uniaxial compressive response of Mix B. (a) Constant strain-rate tests at selected values of the applied strain rate; (b) constant stress creep test and selected values of the applied stress. The predictions of the phenomenological model are also included.

Experimental Results

Monotonic Behavior

The uniaxial constant applied strain and constant stress creep response of mix B (75% by volume sand) are plotted in Figs. 2(a and b), respectively. In the constant strain-rate experiments, the axial stress σ_{33} increases progressively with strain ε_{33}, until a maximum value is attained. Following Deshpande and Cebon (2000), this stress is defined as the "steady-state" stress for the applied strain rate. This steady-state stress increases with increas-

J. Mater. Civ. Eng., 2010, 22(2): 124-135

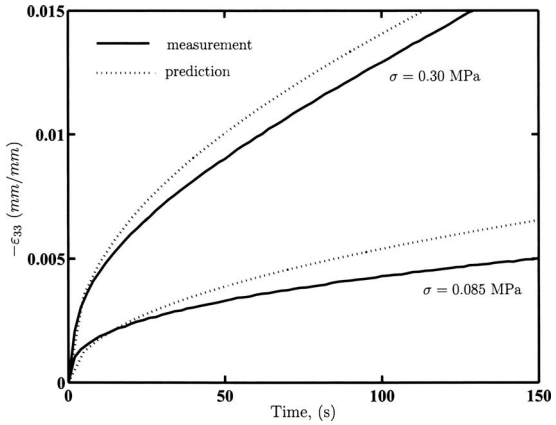

Fig. 3. Triaxial creep tests on Mix B (75% volume fraction) with a stress ratio $\eta=0.6$ for two selected values of the applied deviatoric stress σ. The predictions of the phenomenological model are also included.

ing applied strain rate. The uniaxial constant stress creep response (i.e., the variation of the axial strain ε_{33} with time) for two values of the applied axial stress σ_{33} is plotted in Fig. 2(b). The creep curves comprise a primary creep regime where the strain rate decreases with time, a secondary or steady-state creep regime where the strain-rate $\dot{\varepsilon}_{ss}$ is constant; and a tertiary creep regime [not shown in Fig. 2(b)] where the strain rate increases with increasing time. The steady-state strain rate increases with increasing σ_{33}. The effect of stress triaxiality on the creep response of Mix B is shown in Fig. 3 where the creep response is plotted for $\eta=0.6$ for two values of the deviatoric stress σ. [For a complete set of experimental data under different loading conditions see Ossa (2004)]. Comparing Figs. 2(b) and 3 it can be seen that for a given value of the deviatoric stress σ, the steady-state strain rate decreases with increasing η.

Fig. 4(a) summarizes the monotonic steady-state behavior of Mix B over a range of applied deviatoric stresses σ and stress triaxialities ranging from uniaxial ($\eta=1/3$) to $\eta=1.0$. For the uniaxial stress state ($\eta=1/3$) the steady-state results from both the constant strain rate and constant stress creep tests are included. The results from both the constant strain rate and constant stress creep tests are complimentary with the results overlapping at intermediate values of stress and strain rate [see also Deshpande and Cebon (2000)]. The effect of the hydrostatic stress σ_m on the response of Mix B is seen in Fig. 4(a) with the steady-state axial strain rate $\dot{\varepsilon}_{ss}$ decreasing with increasing η for a given value of σ. The effect of sand volume fraction v_f on the steady-state creep response of the four bitumen/sand mixes investigated here is summarized in Fig. 4(b) for a stress triaxiality $\eta=1/3$. Similar to the findings of Deshpande and Cebon (1999), the steady-state creep resistance of the mixes increases with increased volume fraction of sand. This steady-state creep strain rate versus applied deviatoric stress relationship is well described by an extended Cross model (Cheung and Cebon 1997)

$$\frac{\dot{\varepsilon}_{ss}}{q(\eta)\dot{\varepsilon}_o}=\frac{\sigma}{\sigma_o}\left\{1+\left[\frac{\dot{\varepsilon}_{ss}}{q(\eta)\dot{\varepsilon}_o}\right]^m\right\} \tag{9}$$

where $\dot{\varepsilon}_o$ and σ_o=reference strain rate and stress, respectively, and m=strain rate sensitivity exponent. The reference stress σ_o is taken to be 0.2 MPa in all cases. The reference strain-rate $\dot{\varepsilon}_o$ employed to fit the steady-state data in Fig. 4 is listed in Table 2. The strain-rate sensitivity exponent $m=0.615$ was the same as

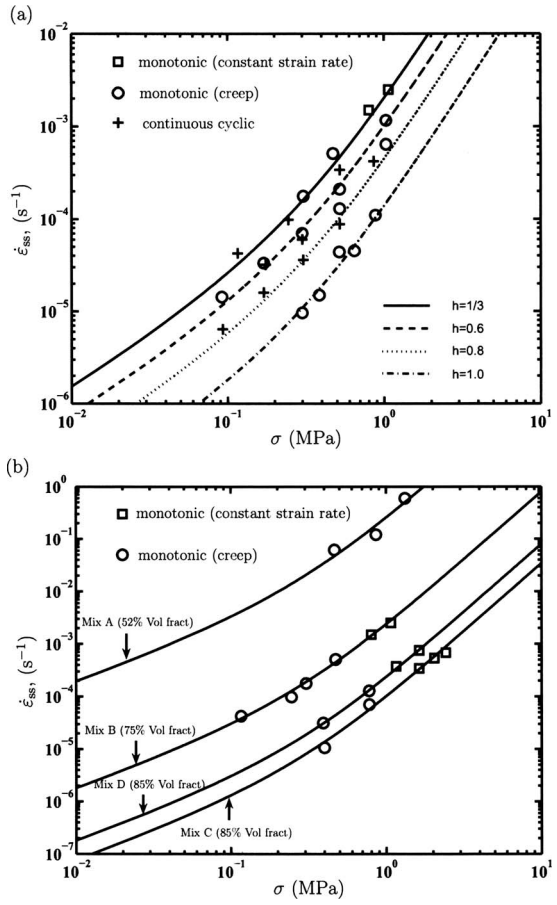

Fig. 4. Monotonic and continuous cyclic steady-state response. (a) Mix B at four values of the stress triaxiality η; (b) the three other mixes investigated in this study.

that of the pure bitumen (Ossa et al. 2005) for all the mixes investigated here. Note that increasing the stress triaxiality does not change the form of the steady-state stress versus strain-rate relationship. Rather increasing η just reduces the steady-state strain rate for a given value of σ. Thus, the effect of the stress triaxiality is adequately captured by introducing the "strengthening" function $q(\eta)$ in Eq. (9). It is useful to calculate the reference strain-rate $\dot{\varepsilon}_o$ using a uniaxial compression test (see later). Thus, by definition $q(\eta=1/3)=1$ with q decreasing with increasing stress triaxiality.

The variation of the measured hydrostatic strain $H=\varepsilon_{33}+2\varepsilon_{11}$ with a measure of the distortional strain $\varepsilon=2/3(\varepsilon_{33}-\varepsilon_{11})$ is plotted in Fig. 5(a) for Mix B at two stress triaxialities $\eta=0.6$ and 0.8. [The strain histories upon unloading are also included in Fig. 5(a).] After an initial compaction, Mix B dilates with a linear relationship between the dilation H and the distortional strain ε with the slope of the H versus $|\varepsilon|$ relation independent of the

Table 2. Dilation Gradients s and Recovery Constants ψ of the Mixes Investigated in This Study

Mix	Dilation gradient s	Recovery constant ψ
Mix A (52%)	≈0	0.45
Mix B (75%)	0.6–0.75	0.32
Mix C (85%)	0.85–1.15	0.17
Mix D (85%)	0.9–1.15	0.17

J. Mater. Civ. Eng., 2010, 22(2): 124-135

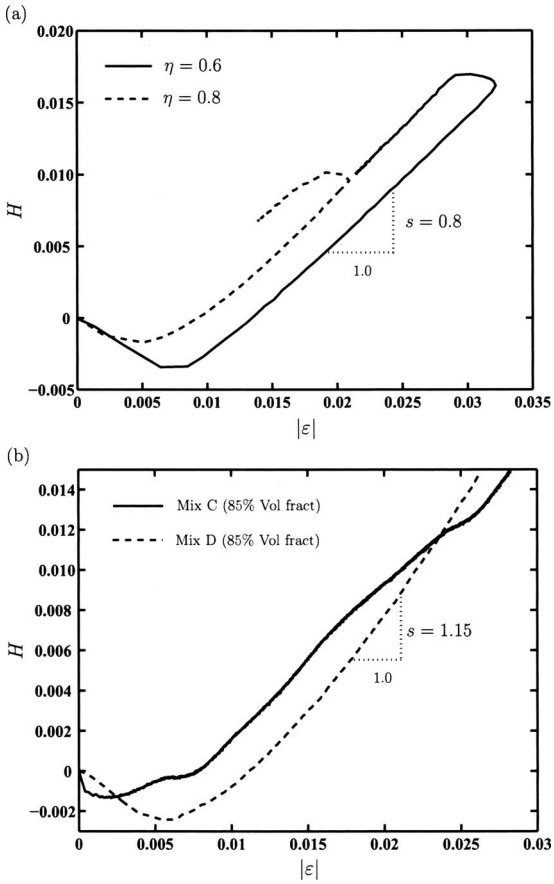

Fig. 5. Variation of the volumetric strain H with distortional strain ε for: (a) Mix B at two values of the stress triaxiality η; (b) Mixes C (made with rounded stones) and D (made with angular stones) under uniaxial compression. The data upon unloading are also included.

value of the applied deviatoric stress σ and stress triaxiality η. This suggests that the dilation is governed by the kinematic constraints imposed by the aggregate skeleton [see Deshpande and Cebon (1999) for a full discussion]. This kinematic constraint can be expressed as

$$H = s|\varepsilon| \tag{10}$$

where s = "dilation gradient" that depends only on aggregate properties.

For example, the dilation gradient of the 85% by volume sand mixes (Mixes C and D) $s \approx 1.15$ [Fig. 5(b)] while $s = 0.85$ for Mix B [Fig. 5(a)]. Interestingly, the dilation gradients for the 85% mixes comprising angular and subspherical aggregate are approximately equal (to within the variation in the experimental measurements). The measured dilation gradients of the four mixes tested in this study are listed in Table 2. It is worth noting here that since the 52% mix (Mix A) is not fully dense, minimal kinematic constraints are imposed by the aggregate on the deformation and the mix deforms at constant volume with $s = 0$.

The effect of the stress triaxiality on the steady-state creep response of the bitumen-sand mixes is summarized in Fig. 6, where the measured value of the strengthening function $q(\eta)$ is plotted against the stress triaxiality η for the four bitumen-sand mixes investigated here. The stress triaxiality has the greatest effect on the 85% mixes (Mixes C and D) with $q \approx 0.005$ at $\eta = 0.8$ while $q = 1$ for all values of η for the 52% mix (Mix A), as expected. The strengthening effect of the hydrostatic pressure on

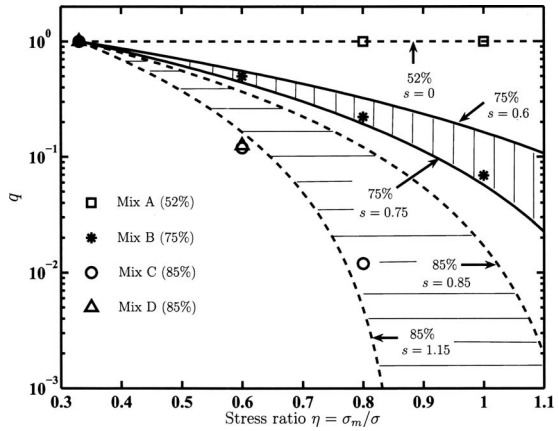

Fig. 6. Strengthening effect q due to the stress triaxiality η for the four mixes investigated in this study. Dashed horizontal lines bound the lower and upper limits of dilatancy s for the 85% volume fraction of aggregate mixes. Dashed vertical lines bound the lower and upper limits of dilatancy s for the 75% volume fraction of aggregate mixes.

the fully dense mixes (i.e., Mixes B, C, and D) is related to the work done by the hydrostatic pressure against the dilation of the mixes as discussed by Deshpande and Cebon (1999). Using a shear-box analogy Deshpande and Cebon (1999) showed that the strengthening function is given by

$$q = \left[\frac{\eta s \ \text{sign}(\sigma) + 1}{1 - s/3} \right]^{1/(1-m)} \tag{11}$$

This prediction has been included in Fig. 6 using the limiting values of the dilation gradients s listed in Table 2 (i.e., two lines bounding the predicted strengthening effect q are plotted in Fig. 6 for both the 75 and 85% mixes). These predictions bound the experimental measurements with reasonable accuracy. In the subsequent analysis, the value of s used will be such that q given by Eq. (11) best fits in the measurements in Fig. 6.

Ossa et al. (2005) showed that the extended Cross model (9) can describe the creep response of pure bitumen over the primary, secondary and tertiary creep regimes, provided the constant reference strain-rate $\dot{\varepsilon}_o$ is replaced by a reference strain-rate $\dot{\varepsilon}_o(\varepsilon_{33})$ that is a function of the axial strain. Thus, the Cross model (9) is generalized as

$$\frac{\dot{\varepsilon}_{33}}{q(\eta)\dot{\varepsilon}_o(\varepsilon_{33})} = \frac{\sigma}{\sigma_o}\left\{ 1 + \left[\frac{\dot{\varepsilon}_{33}}{q(\eta)\dot{\varepsilon}_o(\varepsilon_{33})} \right]^m \right\} \tag{12}$$

This model assumes that for a given mix, $\dot{\varepsilon}_o(\varepsilon_e)q(\eta)$ is a unique function of the strain ε_{33} and independent of the applied loading. This hypothesis is tested here by extracting the function $\dot{\varepsilon}_o(\varepsilon_{33})$ from a series of creep tests on the 75% mix (Mix B) with q given by Eq. (11). These curves, $q\dot{\varepsilon}_o$ versus ε_{33}, are plotted in Fig. 7(a) for several values of η and σ. To within experimental scatter the curves are essentially identical, thus confirming our hypothesis that the creep response of the mix is well described by Eq. (12) over a range of strains, applied deviatoric stresses and stress triaxialities. Note that Eq. (12) also suffices to characterize the creep response of the three other mixes investigated here. The functions $\dot{\varepsilon}_o(\varepsilon_{33})$ for these mixes are plotted in Fig. 7(b).

J. Mater. Civ. Eng., 2010, 22(2): 124-135

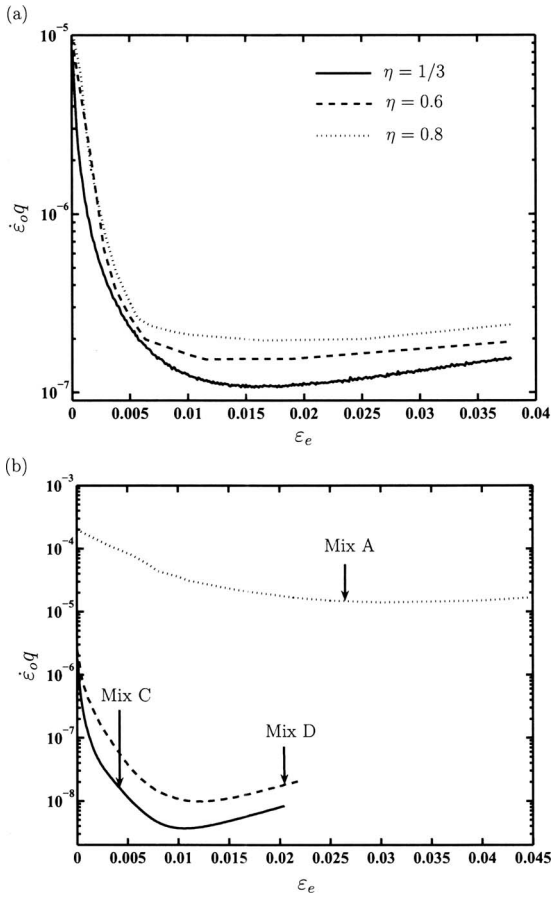

Fig. 7. Calibration curves $\dot{\varepsilon}_o(\varepsilon_e)q$ for the Cross model. (a) $\dot{\varepsilon}_o(\varepsilon_e)q$ for Mix B inferred from creep tests at selected stress triaxialities η; (b) the calibrations curves $\dot{\varepsilon}_o(\varepsilon_e)q$ for the other three mixes investigated in this study.

Creep Recovery Behavior

Creep recovery tests were performed for a range of applied deviatoric stresses σ and stress triaxialities η for unloading from total axial strains ε_{33}^T in the range $0.005 \leq \varepsilon_{33}^T \leq 0.04$. The creep recovery response (axial strain ε_{33} versus time t) of Mix B with $\eta = 1.0$ at two selected values of deviatoric stress σ is plotted in Fig. 8. Similar to the recovery behavior of pure bitumen (Ossa et al. 2005), the recovered strain ε_{33}^r increases with increasing ε_{33}^T. The results from all the creep recovery tests performed on Mix B are summarized in Fig. 9 where the recovered axial strain $\varepsilon_{33}^r \equiv \varepsilon_{33}^T - \varepsilon_{33}^{\text{pl}}$ is plotted as a function of the total axial strain ε_{33}^T prior to unloading; see Eq. (4). The figure reveals that, to within experimental error

$$\varepsilon_{33}^r = \psi \varepsilon_{33}^T \tag{13}$$

with the slope of the line being independent of the stress triaxiality η (for η in the range 1/3 to 1.0). Using the terminology adopted by (Ossa et al. 2005) for pure bitumen, this slope is referred to as "recovery constant" ψ $(0 \leq \psi \leq 1)$. The experimental measurements suggest that $\psi \approx 0.32$ for Mix B (75%). All the mixes investigated here exhibited similar behavior with ψ decreasing with increasing volume fraction of sand; the measured values of ψ for the four mixes tested here are included in Table 2 [see Ossa (2004) for the complete set of experimental results].

Ossa et al. (2005) observed that the unloading or creep recovery rate of pure bitumen was dependent on the recoverable strain.

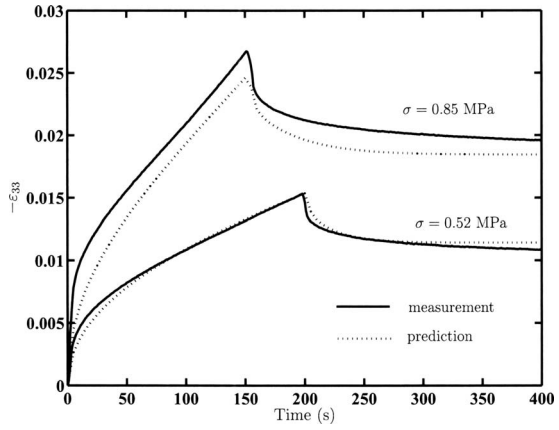

Fig. 8. Creep recovery tests for Mix B with $\eta = 1.0$ for two values of the applied deviatoric stress σ. The predictions of the phenomenological model are also included.

Using the recoverable strain definition of Ossa et al. (2005), the recoverable effective strain in the bitumen-sand mixes is defined as

$$\hat{\varepsilon}_{33}^r = \left(\frac{\varepsilon_{33}}{\varepsilon_{33}^{\text{pl}}} - 1\right)\left(\frac{1-\psi}{\psi}\right) \tag{14}$$

The normalization has been chosen such that $\hat{\varepsilon}_{33}^r = 1$ at the instant of unloading and $\hat{\varepsilon}_{33}^r = 0$ when $\varepsilon_{33} = \varepsilon_{33}^{\text{pl}}$. The creep recovery rates $\dot{\varepsilon}_u(\hat{\varepsilon}_{33}^r)$ are plotted in Fig. 10(a) from tests at selected values of the stress triaxiality η on the 75% mix (Mix B). Note from Fig. 10(a) that the recovery rate $\dot{\varepsilon}_u(\hat{\varepsilon}_{33}^r)$ is a unique function of $\hat{\varepsilon}_{33}^r$ and independent of the loading history. In fact, it is also not affected by the presence of hydrostatic pressure during unloading. For example, creep recovery in the $\eta = 0.6$ and 0.8 tests takes place under a finite hydrostatic pressure as only the axial load is removed during the recovery period. By contrast, creep recovery in the uniaxial creep test $(\eta = 1/3)$ occurs under zero load (no deviatoric or hydrostatic stresses). Similar results are also found for the three other mixes investigated here and their creep recovery curves $\dot{\varepsilon}_u(\hat{\varepsilon}_{33}^r)$ are plotted in Fig. 10(b).

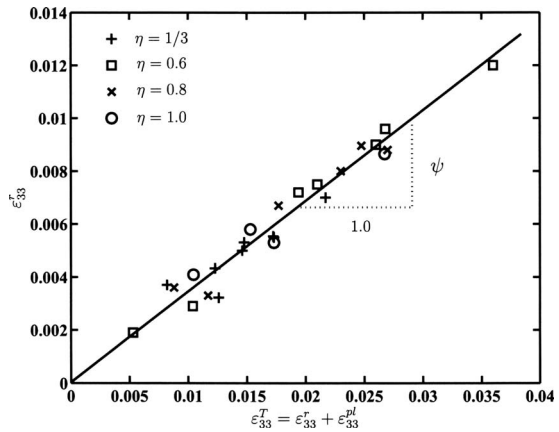

Fig. 9. Summary of the creep recovery experimental results for Mix B showing the linear relationship between the recovered strain and the total applied strain

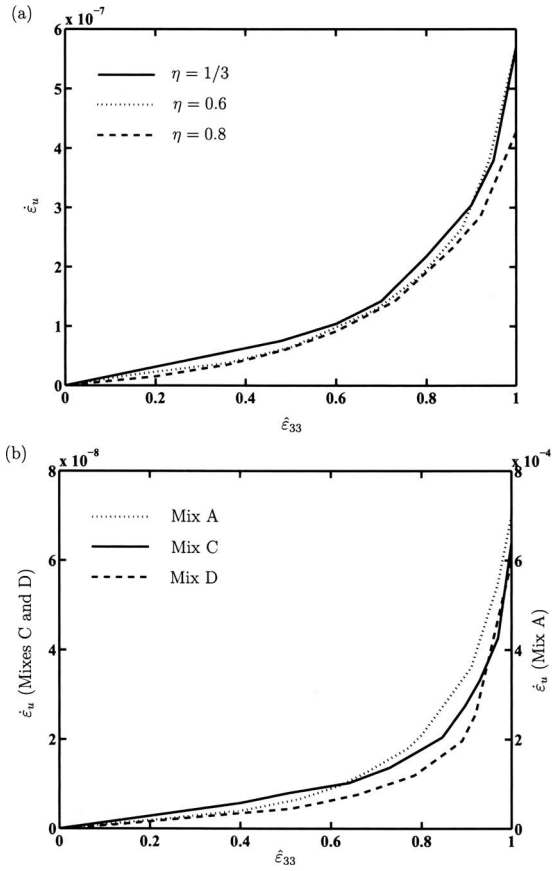

Fig. 10. Recovery calibration curves $\dot{\varepsilon}_u(\hat{\varepsilon}^r_{33})$: (a) for Mix B inferred from recovery tests at selected stress triaxialities η; (b) for the three other mixes investigated in this study

Continuous Cyclic Response

Triaxial stress-controlled continuous cyclic tests [Fig. 1(c)] were performed to investigate the effect on the cyclic strain versus time response of the mixes of the mean cyclic deviatoric stress σ_{mc}, the mean stress triaxiality η_m, the ratio of the maximum to minimum deviatoric stress R, and loading frequency f.

The measured strain versus time response of Mix B with $R=0.7$, a stress triaxiality $\eta_m=0.6$ and loading frequency $f=0.5$ Hz is plotted in Fig. 11 for two values of the mean cyclic deviatoric stress σ_{mc}. The cyclic stress-controlled response is seen to be qualitatively similar to the monotonic creep response (Fig. 3), with primary and secondary creep regimes. The cyclic steady-state strain rate is defined as the average strain rate in the secondary creep regime: analogous to the monotonic creep response, this steady-state strain rate increases with increasing mean cyclic deviatoric stress σ_{mc} for fixed R, f, and η_m.

Next, consider the influence of the loading frequency f and load ratio R on the cyclic creep response, for a given stress triaxiality and mean cyclic deviatoric stress. The measured strain versus time history of Mix B with $\sigma_{mc}=0.52$ MPa, $R=0.7$, and $\eta_m=0.6$ is plotted in Fig. 12(a) for three values of f and in Fig. 12(b) with $\sigma_{mc}=0.18$ MPa, $f=0.5$ Hz, and $\eta_m=0.6$ for two deviatoric stress ratios R. These figures demonstrate that the load ratio R and frequency f have little effect on the cyclic creep response of the mix.

Given that the cyclic creep response of the mix is primarily governed by the mean cyclic deviatoric stress, it is worth examining the relationship between the cyclic and monotonic steady-

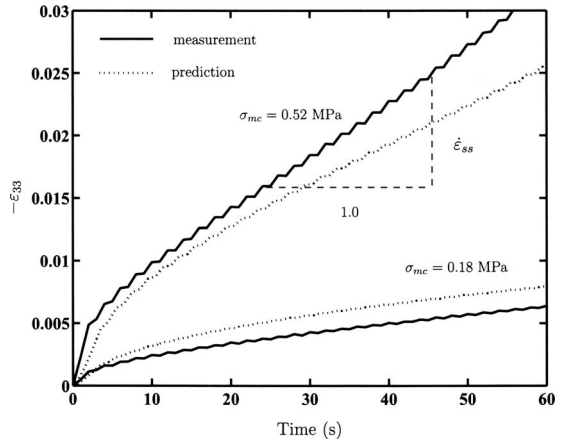

Fig. 11. Continuous cyclic triaxial tests on Mix B. Results are plotted for two values of σ_{mc}, with $f=0.5$ Hz, $\eta_m=0.6$, and $R=0.7$. The predictions of the phenomenological model are also included.

state strain rates of the bitumen-sand mixes. The cyclic steady-state strain rate from a series of tests on Mix B (with varying values of f and R) is plotted in Fig. 4(a) as a function of the mean cyclic deviatoric stress σ_{mc}. Results are plotted in Fig. 4(a) for the

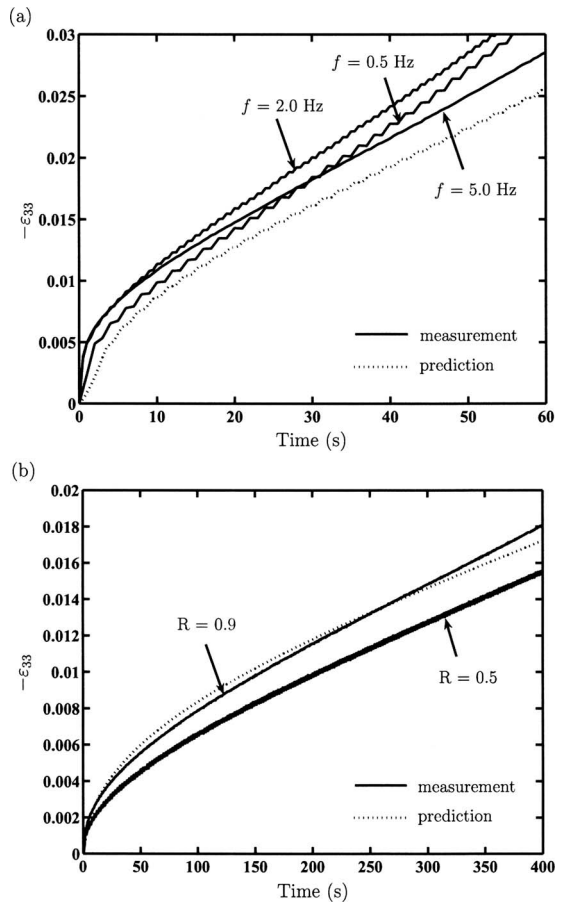

Fig. 12. Continuous cyclic triaxial tests on Mix B. (a) Results for three values of f with $\sigma_{mc}=0.52$ MPa, $\eta_m=0.6$, and $R=0.7$; (b) results for two selected values of R with $\sigma_{mc}=0.18$ MPa, $\eta_m=0.6$, and $f=0.5$ Hz. The predictions of the phenomenological model are also included.

J. Mater. Civ. Eng., 2010, 22(2): 124-135

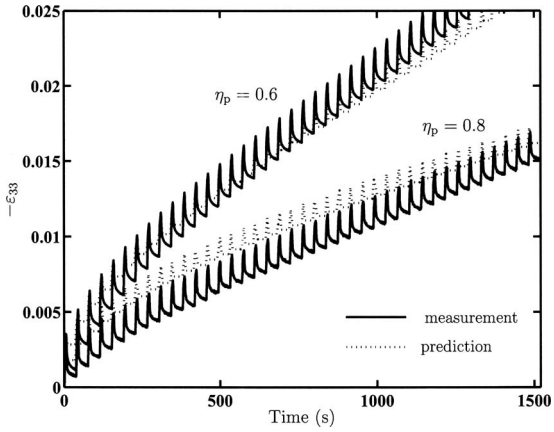

Fig. 13. Triaxial pulse tests on Mix B with σ_p=0.3 MPa, Δ_p=8 s, Δ_g=30 s at two stress ratios η_p. The predictions of the phenomenological model are also included.

four stress triaxialities η considered under monotonic loading with η interpreted as the mean stress triaxiality η_m in the cyclic case. Fig. 4(a) reveals that the cyclic steady-state creep response follows the monotonic response with σ interpreted as σ_{mc} and the stress triaxiality η interpreted as η_m. It is worth mentioning here that the measurements of the radial strains in the continuous cyclic tests showed that the dilation H varied linearly with the distortional strain ε with the dilation gradient s remaining unchanged from the monotonic value (Table 2). This confirms that the dilation is a result of the kinematic constraints due to the aggregate skeleton and is independent of the applied loading. Similar results were also observed from the continuous cyclic creep tests on the three other mixes (Ossa et al. 2004a,b), those results are omitted here for the sake of brevity [see Ossa (2004) for the complete set of experimental results].

Pulse Train Triaxial Behavior

Cyclic stress-controlled pulse tests were performed for a range of deviatoric pulse stresses σ_p, time period ratios Δ_p/Δ_g [see Fig. 1(d)], and stress triaxialities η_p. Representative results for tests on Mix B with a pulse period Δ_p=8 s and a rest period Δ_g=30 s are shown in Fig. 13 for an applied stress σ_p=0.3 MPa and two values of the stress triaxiality η_p=0.6 and 0.8. The results show that for fixed values of σ_p and time periods Δ_p and Δ_g, the accumulated permanent strain decreases with increasing η_p. This is consistent with the monotonic creep results where the creep strain rates decrease with increasing stress triaxiality for a given applied deviatoric stress. However, in contrast to the continuous cyclic creep tests, significant strain recovery is observed during the rest periods between the load pulses. The axial strain versus time measurements from pulse stress tests on the 85% mixes (Mixes C and D) with η_p=0.6 and σ_p=0.52 MPa are plotted in Fig. 14. In these tests the pulse and rest periods were Δ_p=20 s and Δ_g=60 s, respectively. The larger rests periods result in an increased strain recovery compared to the results for Mix B plotted in Fig. 13.

Phenomenological Constitutive Model

A phenomenological model for the triaxial response of the bitumen/sand mixes is proposed here. The model is motivated by the following experimental observations.

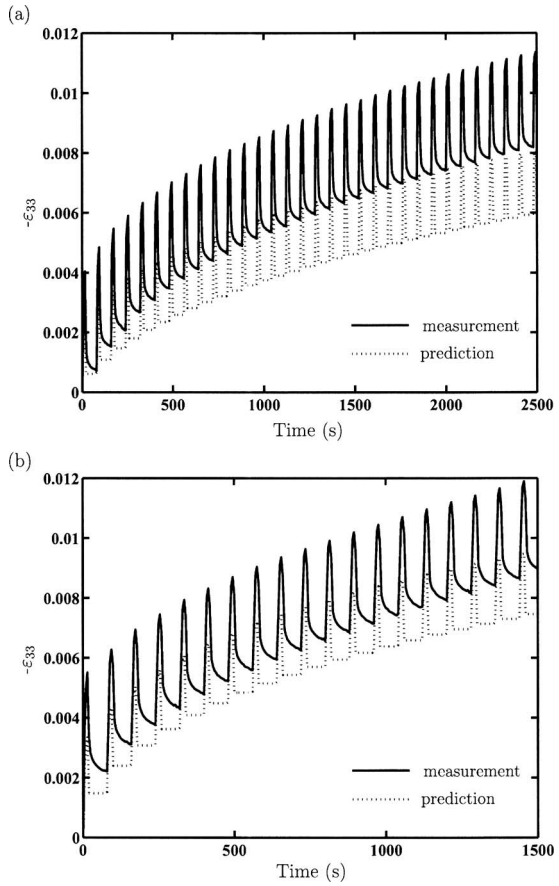

Fig. 14. Triaxial pulse test results on the mixes with 85% by volume aggregate. (a) Mix C (subspherical aggregate) with σ_p=0.52 MPa, Δ_p=20 s, and Δ_g=60 s; (b) Mix D (angular aggregate) with σ_p =0.52 MPa, Δ_p=20 s, and Δ_g=60 s. The predictions of the phenomenological model are also included.

1. The monotonic response is adequately described by an extension of the Cross model, Eq. (12) function of the effective strain ε_e.
2. The kinematic constraints imposed by the aggregate skeleton result in the volumetric strain H being linearly related to the distortional strain ε and independent of the applied loading.
3. The effect of the stress triaxiality on the creep response is adequately modeled by the shear-box model of Deshpande and Cebon (1999). Using this approach, the effect of the stress triaxiality can be simply accounted for by introducing the strengthening effect q in the extended Cross model.
4. The recovery strain rate is independent of the loading history and applied hydrostatic stress. This recovery rate is only a function of the recoverable strain.
5. Negligible strain recovery occurs in the continuous cyclic creep tests with the continuous cyclic creep response almost identical to the monotonic creep response. This suggests that strain recovery only occurs when the applied deviatoric stress is 0.

Adopting Cartesian tensor notation, the total strain-rate $\dot{\varepsilon}_{ij}$ is written as

$$\dot{\varepsilon}_{ij} = \dot{\varepsilon}^e_{ij} + \dot{D}_{ij} \tag{15}$$

where $\dot{D}_{ij}$=inelastic strain rate. The elastic strain rate given by the isotropic Hooke's law as

J. Mater. Civ. Eng., 2010, 22(2): 124-135

$$\dot{\varepsilon}_{ij}^{e} = \frac{1+\nu}{E}\dot{\sigma}_{ij} - \frac{\nu}{E}\dot{\sigma}_{kk}\delta_{ij} \tag{16}$$

where E and ν=Young's modulus and Poisson's ratio, respectively, δ_{ij} the Kronecker delta and $\dot{\sigma}_{ij}$ the applied stress rate. Following Ossa et al. (2005) we write the inelastic strain-rate $\dot{D}_{ij}$ as the sum of the viscous creep rate $\dot{\varepsilon}_{ij}^{v}$ and the recovery rate $\dot{\varepsilon}_{ij}^{r}$ that is active when the deviatoric stresses are 0, that is

$$\dot{D}_{ij} = \dot{\varepsilon}_{ij}^{v} + \dot{\varepsilon}_{ij}^{r} \tag{17}$$

Employing the observation that the volumetric strain is linearly related to the distortional strain via Eq. (10), the viscous creep rate is written as the sum of the deviatoric and volumetric components as

$$\dot{\varepsilon}_{ij}^{v} = \frac{1}{1-s/3}\left[\frac{3}{2}\frac{\sigma_{ij}^{d}}{\sigma_{e}}\dot{\varepsilon}_{e}^{v} + \frac{s\dot{\varepsilon}_{e}^{v}}{3}\delta_{ij}\right] \tag{18}$$

Here $\sigma_{ij}^{d} \equiv \sigma_{ij} - \sigma_{kk}/3$ is the deviatoric stress and $\sigma_{e} \equiv \sqrt{3/2\sigma_{ij}^{d}\sigma_{ij}^{d}}$ is the von Mises effective stress. Note that the factor $(1-s/3)$ has been introduced in Eq. (18) so that the effective viscous strain-rate $\dot{\varepsilon}_{e}^{v}$ is equal to the axial strain rate in a uniaxial compression test. With $\varepsilon_{e}^{v} = \varepsilon_{33}^{v}$ in a uniaxial compression test, we can replace ε_{33} in Eq. (12) by ε_{e} and thus this equivalent strain rate is given by the extended Cross model as

$$\dot{\varepsilon}_{e}^{v} \equiv \frac{\dot{\varepsilon}_{e}^{\mathrm{pl}}}{1-\psi} = \frac{q(\omega)\sigma_{e}\dot{\varepsilon}_{o}(\varepsilon_{e})}{\sigma_{o}}\left\{1 + \left[\frac{\dot{\varepsilon}_{e}^{v}}{q(\omega)\dot{\varepsilon}_{o}(\varepsilon_{e})}\right]^{m}\right\} \tag{19a}$$

where

$$q(\omega) = \left(\frac{s\omega+1}{1-s/3}\right)^{1/(1-m)} \tag{19b}$$

and $\omega \equiv \sigma_{kk}/\sigma_{e}$ is the three-dimensional equivalent of the axisymmetric stress triaxiality η. It is worth noting that here we follow Ossa et al. (2005) and specify that $\dot{\varepsilon}_{o}$ is a function of the total effective strain ε_{e} given by

$$\dot{\varepsilon}_{e} = \dot{\varepsilon}_{e}^{v} + \dot{\varepsilon}_{e}^{r} \tag{20}$$

where $\dot{\varepsilon}_{e}^{r}$ is the effective recovery strain rate. The recovery rate is also decomposed into deviatoric and volumetric components as

$$\dot{\varepsilon}_{ij}^{r} = \frac{1}{1-s/3}\left[\dot{\varepsilon}_{e}^{r}\frac{\varepsilon_{ij}^{d}}{D_{e}} + \frac{s\dot{\varepsilon}_{e}^{r}}{3}\delta_{ij}\right] \tag{21}$$

where the deviatoric strain $\varepsilon_{ij}^{d} \equiv D_{ij} - D_{kk}/3$ and the effective strain $D_{e} \equiv \sqrt{2/3\varepsilon_{ij}^{d}\varepsilon_{ij}^{d}}$. Similar to the viscous strain rate, the $(1-s/3)$ factor ensures that $\dot{\varepsilon}_{e}^{r}$ is the axial recovery rate in an uniaxial compression creep recovery experiment. This recovery rate is independent of the imposed hydrostatic stress and is active only when no deviatoric stresses are applied. Thus, we specify that the effective recovery rate is given by

$$\dot{\varepsilon}_{e}^{r} = -[1 - \mathrm{sign}(\sigma_{e})]\dot{\varepsilon}_{u}(\hat{\varepsilon}_{e}^{r}) \tag{22}$$

where $\dot{\varepsilon}_{u}$ is the axial recovery rate in an uniaxial compressive creep recovery experiment. The normalized recoverable strain $\hat{\varepsilon}_{e}^{r}$ is defined analogously to Eq. (14) as

$$\hat{\varepsilon}_{e}^{r} = \left(\frac{\varepsilon_{e}}{\varepsilon_{e}^{\mathrm{pl}}} - 1\right)\left(\frac{1-\psi}{\psi}\right) \tag{23}$$

and thus $\hat{\varepsilon}_{e}^{r} = \hat{\varepsilon}_{33}^{r}$ in an uniaxial compressive creep recovery test. The constitutive description can be completed by specifying the temperature dependence of the response of the bituminous mixes.

As previously noted by Deshpande and Cebon (2000), the temperature dependence of bituminous mixes follows that of the pure bitumen. For temperatures above the glass transition of bitumen this dependence is governed by activation energy and given by the Arrhenius relations (Ossa et al. 2005)

$$\dot{\varepsilon}_{o}(\varepsilon_{e}) = \dot{\varepsilon}_{oc}(\varepsilon_{e})\exp\left[-k\left(\frac{1}{T} - \frac{1}{273}\right)\right] \tag{24a}$$

and

$$\dot{\varepsilon}_{u}(\hat{\varepsilon}_{e}^{r}) = \dot{\varepsilon}_{uc}(\hat{\varepsilon}_{e}^{r})\exp\left[-k\left(\frac{1}{T} - \frac{1}{273}\right)\right] \tag{24b}$$

where $\dot{\varepsilon}_{oc}$ and $\dot{\varepsilon}_{uc}$=reference strain-rate values at 0°C; T =temperature in Kelvin (K); and k=Arrhenius constant is approximately equal to 23×10^{3} K for the 50 pen bitumen employed in this investigation.

Calibration

The number of constants in this phenomenological model for bitumen-sand mixes is just one more than that in the pure bitumen constitutive model of Ossa et al. (2005); pure bitumen deforms at constant volume while the dilation gradient s of the bitumen-sand mix, that depends on the aggregate skeleton, needs to be additionally measured. The calibration of the constitutive model proposed here involves the following uniaxial compression experiments for a given bitumen-sand mix.

1. Determine the constants in the Cross model m, σ_{o}, and $\dot{\varepsilon}_{o}(\varepsilon_{e})$ via a series of uniaxial compression experiments.
2. Determine the recovery constant ψ and recovery rate $\dot{\varepsilon}_{u}(\hat{\varepsilon}_{e}^{r})$ from a uniaxial compressive creep recovery experiment.
3. Measure the dilation gradient s from a uniaxial compression experiment.

The Arrhenius constant which gives the temperature dependence of the mix is assumed to be known for the pure bitumen used in the mix. However, this constant can easily be determined by performing uniaxial compression experiments on the mixes at two selected temperatures, as described by Ossa et al. (2005).

We note that many experimental investigations have shown that the void content and its distribution have a significant effect on the deformation behavior of bitumen/aggregate mixes (Von Quintus et al. 1991; Murali Krishnan and Rao 2000; Murali Krishnan and Rajagopal 2004). In the phenomenological model proposed here, the void content, its distribution and evolution with deformation are implicitly taken into account in the loading and recovery calibration curves $\dot{\varepsilon}_{o}(\varepsilon_{e})$ and $\dot{\varepsilon}_{u}(\hat{\varepsilon}_{e}^{r})$ for a given mix and thus need not be considered separately.

Comparison with Experimental Results

Comparisons between model predictions and experimental results for the monotonic constant strain rate and constant stress creep tests are shown in Figs. 2 and 3, while comparisons with the creep recovery tests are presented in Fig. 8. Similarly, comparisons with the continuous cyclic experiments are shown in Figs. 11 and 12. [Note that the phenomenological model predicts a continuous stress-controlled cyclic response that is only dependent on σ_{mc} and η_{m} for a given mix and thus only a single prediction curve is included in Figs. 12(a and b)]. All these comparisons are for Mix B with 75% by volume sand; comparisons of the model with measurements from the three other mixes investigated here are

J. Mater. Civ. Eng., 2010, 22(2): 124-135

omitted for the sake of brevity [see Ossa (2004) for the complete set of experimental results]. However, it is worth noting that good agreement between the measurements and model predictions was also observed in all cases (Ossa et al. 2004a,b).

A key judge of the accuracy of the model lies in its ability to predict the response of the mixes in the pulse loading tests. In these tests both the creep response under load and the recovery behavior is combined in a complicated manner. Such comparisons for pulse loading tests on mix B (75% by volume sand) at two selected stress triaxialities η_p are shown in Fig. 13. Similarly, comparisons between the measurements and predictions of the pulse train responses of Mixes C and D are shown in Figs. 14(a and b), respectively. The model predicts the total accumulated strains with reasonable accuracy in all these cases. The accumulated strain in pulse stress tests is the relevant parameter in predicting the rutting response of a pavement. It is important to emphasize here that the differences seen between the model predictions and experimental results are strongly influenced by experimental scatter (primarily due to manufacturing variabilities between different specimens).

The model proposed here is thus seen to be capable of predicting the response of bitumen/aggregate mixes ranging from 52 to 85% volume fractions of aggregate under the monotonic and cyclic triaxial loading conditions studied. The model is simple to calibrate and does not involve determining a relaxation spectrum for the mix as required by most of the models described in the literature.

Conclusions

The triaxial compressive response of bituminous mixes with volume fractions of aggregate in the range 52 to 85% was investigated over a wide range of stresses and strain rates. The types of loading histories considered include monotonic constant applied strain rate and constant stress as well as creep recovery, continuous cyclic, and stress pulse stress loadings. The temperature dependence of the mixes of aggregate and bitumen was governed by the temperature dependence of the bitumen [see for example Deshpande and Cebon (2000) and Ossa (2004)].

1. The fully dense mixes with a volume fraction of aggregate greater than 64% dilate under all loading conditions and the creep responses of these mixes depends on both the deviatoric and hydrostatic stresses.
2. The creep resistance of the mixes increases with increasing volume fraction of aggregate, though the angularity of the aggregate has only a minor effect on the creep strength of the mixes.
3. Creep recovery occurs under states of 0 deviatoric stresses and the recovery rate is observed to be reasonably independent on any applied hydrostatic stress.
4. Under continuous stress-controlled cyclic loading, the creep rate of the mixes is mainly governed by the applied mean cyclic stress; with this mean cyclic stress interpreted as the constant applied stress in a monotonic creep test, the cyclic and monotonic responses of the mixes are almost identical. By contrast, if rest periods exist between the applied stress pulses the average creep rate is significantly affected by the creep recovery during the rest periods.
5. A phenomenological constitutive model for the multiaxial response of the bituminous mixes is proposed. This model can be calibrated by uniaxial compression creep and recovery experiments. This simple model is shown to adequately capture the measured responses of the mixes over the wide range of loadings situations considered here.

Acknowledgments

Support from the Nottingham Asphalt Research Consortium (NARC) is gratefully acknowledged. The writers would also like to thank Shell Bitumen U.K. for supply of the materials studied.

References

Abbas, A. R., Papagiannakis, A. T., and Masad, E. A. (2004). "Linear and nonlinear viscoelastic analysis of the microstructure of asphalt concretes." *J. Mater. Civ. Eng.*, 16(2), 133–139.

Brown, S. F., and Cooper, K. E. (1980). "A fundamental study of the stress-strain characteristics of a bituminous material." *Proc., Association of Asphalt Paving Technologists*, Vol. 49, 476–498.

Brown, S. F., and Snaith, M. S. (1974). "The permanent deformation characteristics of a dense bitumen macadam subjected to repeated loading." *Proc., Association of asphalt Paving Technologists*, Vol. 45, 224–252.

Chang, G. K., and Meegoda, N. J. (1993). "Simulation of the behaviour of asphalt concrete using discrete element method." *Proc, 2nd Int. Conf. on Discrete Element Methods*, Massachusetts Institute of Technology, Cambridge, Mass., 437–448.

Cheung, C. Y. (1995). "Mechanical behaviour of bitumens and bituminous mixes." Ph.D. thesis, Cambridge Univ., Engineering Dept.

Cheung, C. Y., and Cebon, D. (1997). "Experimental study of pure bitumens in tension, compression, and shear." *J. Rheol.*, 41(1), 45–73.

Cheung, C. Y., Cocks, A. C. F., and Cebon, D. (1999). "Isolated contact model of an idealized asphalt mix." *Int. J. Mech. Sci.*, 41, 767–792.

Collop, A. C., and Khanzada, S. (2001). "Permanent deformation in idealised 'sand asphalt' bituminous mixtures." *Road Mater. Pavement Des.*, 2(1), 7–28.

Collop, A. C., Scarpas, A., Kasbergen, C., and de Bondt, A. (2003). "Development and finite element implementation of stress-dependent elastoviscoplastic constitutive model with damage for asphalt." *Transportation Research Record. 1832*, Transportation Research Record, Washington, D.C., 96–104.

Deshpande, V. S., and Cebon, D. (1999). "Steady-state constitutive relationship for idealised asphalt mixes." *Mech. Mater.*, 31, 271–287.

Deshpande, V. S., and Cebon, D. (2000). "Uniaxial experiments on idealised asphalt mixes." *J. Mater. Civ. Eng.*, 12(3), 262–271.

German, R. M. (1989). *Particle packing characteristics*, Metal Powder Industries Federation, Princeton, N.J.

Hills, J. F., and Heukelom, W. (1969). "The modulus and Poisson's ratio of asphalt mixes." *J. Inst. Pet.*, 55(541), 27–35.

Huang, B., Mohammad, L., and Wathugala, G. (2002). "Development of a thermo-viscoplastic constitutive model for HMA mixtures." *Electron J. Assoc. Asph. Paving Technol.*, 71, 594–618.

Huang, B., Mohammad, L., and Wathugala, G. (2004). "Application of a temperature dependent viscoplastic hierarchical single surface model for asphalt mixtures." *J. Mater. Civ. Eng.*, 16(2), 147–154.

Huang, Y. H. (1967). "Stresses and displacements in viscoelastic layered systems under circular loaded areas." *Proc., 2nd Int. Conf. on the Structural Design of Asphalt Pavements*, 225–244.

Lee, H., and Kim, Y. R. (1998). "Viscoelastic constitutive model for asphalt concrete under cyclic loading." *J. Eng. Mech.*, 124(1), 32–40.

Long, F. M. (2001). "Permanent deformation of asphalt concrete pavements: A nonlinear viscoelastic approach to mix analyses and design." Ph.D. thesis, Univ. of California, Berkeley.

Lytton, R., Uzan, J., Fernando, E. G., Roque, R., Hiltunen, D. and Stoffels, S. M. (1993). "Development and validation of performance prediction models and specifications for asphalt binders and paving

mixes." *Technical Rep. No. SHRP-A-357*, Strategic Highway Research Program, National Research Council.

Murali Krishnan, J., and Rajagopal, K. R. (2004). "Thermodynamic framework for the constitutive modeling of asphalt concrete: Theory and applications." *J. Mater. Civ. Eng.*, 16(2), 155–166.

Murali Krishnan, J., and Rao, L. C. (2000). "Air void reduction of asphalt concrete using mixture theory." *Int. J. Eng. Sci.*, 38, 1331–1354.

Nijboer, L. J. (1948). *Plasticity as a factor in the design of dense bituminous road carpets*, Elsevier Science, New York.

Ossa, E. A. (2004). "Deformation behaviour of bitumen and bituminous mixes." Ph.D. thesis, Cambridge Univ., Engineering Dept.

Ossa, E. A., Deshpande, V. S., and Cebon, D. (2004a). "Triaxial deformation behaviour of bituminous mixes." *Technical Rep. CUED/C-MICROMECH/TR.96*.

Ossa, E. A., Deshpande, V. S., and Cebon, D. (2004b). "Uniaxial monotonic and cyclic behaviour of bituminous mixes." *Technical Rep. CUED/C-MICROMECH/TR.95*.

Ossa, E. A., Deshpande, V. S., and Cebon, D. (2005). "Phenomenological model for the monotonic and cyclic behaviour of pure bitumen." *J. Mater. Civ. Eng.*, 17(2), 188–197.

Ramsamooj, D. V., Ramadan, J., and Lin, G. S. (1998). "Model prediction of rutting in asphalt concrete." *J. Transp. Eng.*, 124(5), 448–446.

Schapery, R. A. (1984). "Correspondence principles and a generalised J integral for large deformation and fracture analysis of viscoelastic media." *Int. J. Fract.*, 25, 195–223.

Von Quintus, H. L., Scherocman, J. A., Hughes, C., and Kennedy, T. (1991). "Asphalt aggregate mixture analysis system." *Technical NCHRP Rep. No. 338*, Transportation Research Board, Washington, D.C.

Whiteoak, D. 1990. *The Shell bitumen handbook*, Shell Bitumen, U.K.

Zhao, Y., and Kim, Y. R. (2003). "Time-temperature superposition for asphalt mixtures with growing damage and permanent deformation in compression." *Transportation Research Record. 1832*, Transportation Research Board, Washington, D.C., 161–172.

Zhu, H., and Nodes, J. E. (2000). "Contact based analysis of asphalt pavement with the effect of aggregate angularity." *Mech. Mater.*, 32, 193–202.